Energy Demand Prediction in Hybrid Electrical Vehicles for Speed Optimization

Daniel Fink[1], Sean Shugar[1], Zygimantas Ziaukas[1], Christoph Schweers[2], Ahmed Trabelsi[2] and Hans-Georg Jacob[1]

[1]*Leibniz University Hannover, Institute of Mechatronic Systems, An der Universität 1, Garbsen, Germany*

[2]*IAV GmbH, Berlin, Germany*

Keywords: Systems Modeling, Energy Demand Prediction.

Abstract: Targeting a resource-efficient automotive traffic, modern driver assistance systems include speed optimization algorithms to minimize the vehicle's energy demand, based on predictive route data. Within these algorithms, the required energy for upcoming operation points has to be determined. This paper presents a model-based approach, to predict the energy demand of a parallel hybrid electrical vehicle, which is suitable to be used in speed optimization algorithms. It relies on separate models for the individual power train components, and is identified for a real test vehicle. On route sections of 5 to 7 km the averaged root mean square error for the state of charge prediction results to 0.91 % while the required amount of fuel can be predicted with an averaged root mean square error of 0.05 liters.

1 INTRODUCTION

A sustainable and resource-efficient mobility is a key challenge in reducing global warming. Intending to meet this demand, the development of vehicles with the lowest possible energy consumption is targeted by manufacturers. Besides physical influences, such as driving resistances, power train system and engine characteristics, the vehicle's energy demand depends significantly on the driver's behavior (Radke, 2013). In this respect, increasing automation of the vehicle control offers high potential to reduce the energy demand. Therefore, considering the energy demand within automated or assisted vehicle control algorithms is of particular importance to increase the resource efficiency in automotive road transport (Rosenzweig and Bartl, 2015).

Energy efficient driving automation is part of current research (Hülsebusch, 2018). A common approach is to plan and optimize a vehicle's speed trajectory for the upcoming route section. Usually, a dynamic programming algorithm (Bellman, 2003) is used for the the optimization process. In this process, an energy model of a vehicle is called to determine the energy requirements based on predictive route data. Within such an optimization procedure, (Radke, 2013) uses a prediction model for a combustion engine vehicle to develop a driver assistance system for the vehicle speed. Test drives indicate the fuel consumption to be reduced by 10.2% when using this system. (Freuer, 2016) demonstrates energy savings of up to 6% when optimizing the vehicle speed using an energy demand model for an electric vehicle. Applying this approach within a risk-sensitive nonlinear model predictive controller (Sajadi-Alamdari et al., 2020) show that the energy efficiency of an electric vehicle can be increased by 21%.

However, there is no investigation of other, more complex drive concepts, such as parallel hybrid electrical drives, to be used within a speed optimization procedure described above. For these drives, literature provides many research works on energy management strategies (Zhang et al., 2020). Unfortunately, these strategies are not suited to be applied directly for any planning and optimizing approaches, as they are usually based on adjusting the torque distribution. According to (Hülsebusch, 2018), this adjustment is not possible in every assistant system. In addition, the proposed strategies are mostly based on vehicle simulations and are not verified under real conditions. An approach that aims to predict the energy demand of hybrid electrical vehicles with a series drive configuration is presented by (Fiori et al., 2018). However, parallel drive configurations, which are characterized by a complex torque distribution mechanism, are not considered. Furthermore, (Pi-

Fink, D., Shugar, S., Ziaukas, Z., Schweers, C., Trabelsi, A. and Jacob, H.
Energy Demand Prediction in Hybrid Electrical Vehicles for Speed Optimization.
DOI: 10.5220/0011075600003191
In *Proceedings of the 8th International Conference on Vehicle Technology and Intelligent Transport Systems (VEHITS 2022)*, pages 116-123
ISBN: 978-989-758-573-9; ISSN: 2184-495X
Copyright © 2022 by SCITEPRESS – Science and Technology Publications, Lda. All rights reserved

tanuwat et al., 2019) presents a hybrid vehicle energy consumption model which only aims to determine the consumed amount of fuel.

In this paper, we present a model based approach to predict the energy demand of a hybrid electrical vehicle with parallel working engines, based on route data. This approach can be used within speed optimization algorithms in driver assistance systems that are not intended to be able to adjust the torque distribution. We build individual models for the single power train components, such as combustion engine, electric motor and battery as well as for the behavior of the gearbox and the torque distribution control. The model approaches are validated for a Volkswagen Golf VII GTE using measured CAN data.

The paper is organized as follows. In section 2 we present the developed energy demand prediction approach, introduce the separate models and demonstrate the identification process. In section 3 the presented approach is validated. Finally our results are concluded in section 4.

2 ENERGY DEMAND MODELING

Algorithms to optimize a speed trajectory often rely on dividing the global optimization problem into smaller sub-problems. Usually, the solution space is discretized and the optimal speed is determined only for the transition between two discrete route points. Previous vehicle states can not be taken into account. Hence, it is required that the energy demand can be determined only relying on the information of two operation points. Therefore, the input values for an energy demand model, which is suitable for common speed optimization algorithms, are limited to distance Δd_k between two discrete operating points, as well as to the velocities v_k, v_{k-1} and the route data based heights h_k, h_{k-1} at both points.

2.1 Model Structure

Using a longitudinal vehicle model, as described in (Mitschke and Wallentowitz, 2004), the required drive wheel torque $T_{\mathrm{w},k}$ to transit from operation point $k-1$ to operation point k can be calculated for a given dynamic rolling radius r_d as follows:

$$T_{\mathrm{w},k}(\alpha_k, a_k, \bar{v}_k) = r_\mathrm{d} \cdot (F_{\mathrm{a},k} + F_{\mathrm{r},k} + F_{\mathrm{g},k} + F_{\mathrm{i},k}). \quad (1)$$

The road slope α_k and the occurring acceleration a_k are derived from the input information, by:

$$\alpha_k = \arctan \frac{h_k - h_{k-1}}{\Delta d_k}, \quad (2)$$

$$a_k = \frac{(v_k - v_{k-1})^2 + 2 \cdot v_{k-1} \cdot (v_k - v_{k-1})}{2 \cdot \Delta d_k}. \quad (3)$$

Furthermore, $\bar{v}_k$ represents the average speed within the transition between the operation points. The driving resistance forces, such as the aerodynamic drag force $F_{\mathrm{a},k}$, the gradient force $F_{\mathrm{g},k}$, the rolling resistance force $F_{\mathrm{r},k}$ and the inertia force $F_{\mathrm{i},k}$ can be determined, based on the defined input information and known vehicle parameters, as follows:

$$F_{\mathrm{a},k} = \frac{1}{2} \rho \cdot c_\mathrm{d} \cdot A_\mathrm{f} \cdot \bar{v}_k^2, \quad (4)$$

$$F_{\mathrm{g},k} = m_\mathrm{v} \cdot g \cdot \sin \alpha_k, \quad (5)$$

$$F_{\mathrm{r},k} = c_\mathrm{r} \cdot m_\mathrm{v} \cdot g \cdot \cos \alpha_k, \quad (6)$$

$$F_{\mathrm{i},k} = m_\mathrm{v} \cdot e_\mathrm{r} \cdot a_k. \quad (7)$$

Here, ρ is the density of air, c_d the aerodynamic drag coefficient, A_f the vehicle frontal area, g the gravitational acceleration, m_v the vehicle mass, c_r the rolling resistance coefficient, and e_r an additional factor to consider rotational masses.

In parallel hybrid electrical power trains, the torque, applied by the two individual engines, cannot be derived from the required wheel torque directly. This torque additionally relies on the behavior of two preconnected components. First, the gearbox which

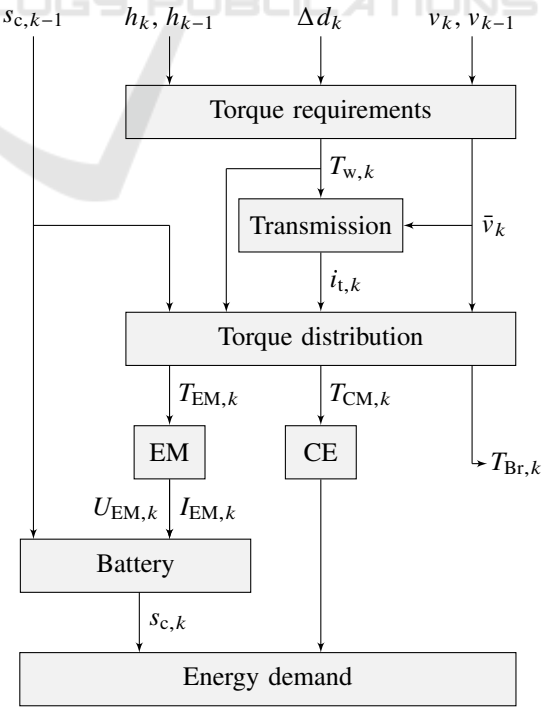

Figure 1: Structure of the prediction approach.

determines the transmission ratio between wheel axle and output shaft of the engines. Second, the torque distribution control which determines the part of total drive torque the single engines are required to apply. The behavior of these components depend on various unpredictable factors, such as the engine temperature. Due to the limited input information within a speed optimization procedure, these components cannot be modeled in detail. However, their behavior must be taken into account when predicting the particular torque and thus the energy demand of the individual drives. For this reason, we present an estimation approach for both, transmission ratio and torque distribution before modeling the electric motor and the combustion engine. The structure of our overall approach to predict the energy demand is demonstrated in figure 1.

2.1.1 Transmission Estimation

The gear selection within the gearbox mainly depends on the drive shaft speed and the torque to be transmitted. As the these values are unknown at this stage of the energy demand model (see figure 1), we aim to estimate a transmission factor $i_{\mathrm{t},k}$ based on vehicle speed $\overline{v}_k$ and wheel torque $T_{\mathrm{w},k}$. Therefore, according to (Nelles, 2001), we declare $i_{\mathrm{t},k}$ for an operation point k to be a linear combination of weighted basis functions, as follows:

$$i_{\mathrm{t},k}(T_{\mathrm{w},k},\overline{v}_k) = \sum_{i=1}^{M_\mathrm{t}}\sum_{j=1}^{N_\mathrm{t}} w_{\mathrm{t},i,j}\Phi_i(T_{\mathrm{w},k},\xi_i)\Phi_j(\overline{v}_k,\eta_j). \quad (8)$$

A basis function $\Phi_q(u,\boldsymbol{c})$ for the input u and a set of grid points $\boldsymbol{c}$ is defined to be a linear function that equals 1 at a grid point c_q while it is 0 at the neighboring c_{q-1} and c_{q+1} and all other grid points, as declared by:

$$\Phi_q(u,\boldsymbol{c}) = \begin{cases} \frac{u-c_{i-1}}{c_i-c_{i-1}}, & \text{if } c_{i-1} \le u \le c_i \\ \frac{u-c_{i+1}}{c_i-c_{i+1}}, & \text{if } c_i < u \le c_{i+1} \\ 0, & \text{otherwise.} \end{cases} \quad (9)$$

In order to determine the weights $w_{\mathrm{t},i,j}$ in equation (8) and thus, to identify the transmission behavior of our test vehicle, we define $M_\mathrm{t} = 23$ grid points ξ_i for the drive wheel torque T_w and $N_\mathrm{t} = 21$ grid points η_j for the vehicle speed $\overline{v}$.

We measure standard CAN data of the test vehicle in drive sequences of 5 to 7 km and create a data set of 525 km in total which consists of $L = 293,512$ measured operating points for the drive shaft speed n^*_d, the vehicle speed v^*, the total power train torque T^*_t, the electric motor torque T^*_EM, the electric motor current I^*_EM, the electric motor voltage U^*_EM, the battery current I^*_B, the battery voltage U^*_B and the battery's state of charge (SOC) s^*_c. Based on this data, the drive wheel torque can be calculated using equation (1) and the actual transmission factor $i^*_{\mathrm{t},k}$ for a single data point k can be approximated by

$$i^*_{\mathrm{t},k} = \frac{n^*_{\mathrm{d},k}}{n_{\mathrm{w},k}} = \frac{2\cdot\pi\cdot r_\mathrm{d}\cdot n^*_{\mathrm{d},k}}{60\cdot v^*_k}. \quad (10)$$

Taking this transmission factor for given data points, a least square algorithm, as described in (Nelles, 2001), is used to determine a optimal set of weights $\boldsymbol{w}_{\mathrm{t,opt}}$ by

$$\boldsymbol{w}_{\mathrm{t,opt}} = \arg\min_{\boldsymbol{w}} \frac{1}{L}\sum_{k=1}^{L}(i_{\mathrm{t},k} - i^*_{\mathrm{t},k})^2, \quad (11)$$

for an identification data set containing about 83 % of the driving sequences in the data set.

2.1.2 Torque Distribution

Using the estimated transmission factor, the required total drive or breaking torque T_t can be derived from the wheel torque. The total drive torque is applied either by a single or by a combination of two power train components such as electric motor, combustion engine and braking system. In order to estimate how the different components are addressed, we introduce a torque distribution estimation approach. We define this estimation to cover all procedures of distributing the required drive torque to the individual drives.

The components to be addressed differ for the states driving or decelerating. In driving state, the required torque is applied through the electric motor, the combustion engine or by a combination of both. In case of decelerating or braking the required torque is a combination of the electric motor's recuperative torque and a braking torque at the wheels. For this reason, we consider the states driving and decelerating separately.

Decelerating State. As the recuperating ability is limited, the required torque can be applied only to a certain extend by the electric motor when decelerating. The remaining part of the required deceleration torque must be applied through the braking system. In order to model this behavior, the method described in section 2.1.1 is used. At deceleration states the electric motor's recuperative torque $T_{\mathrm{EM},k}(T_{\mathrm{t},k}, s_{\mathrm{c},k})$ is assumed to rely on the total required torque $T_{\mathrm{t},k}$, as well as on the battery's SOC $s_{\mathrm{c},k}$:

$$T_{\mathrm{EM},k}(T_{\mathrm{t},k}, s_{\mathrm{c},k}) = \sum_{i=1}^{M_\mathrm{EM}}\sum_{j=1}^{N_\mathrm{EM}} w_{\mathrm{EM},i,j}\Phi_i(T_{\mathrm{t},k},\xi_i)\Phi_j(s_{\mathrm{c},k},\eta_j) \quad (12)$$

We define $M_{\mathrm{EM}} = 7$ grid points for the total torque and $N_{\mathrm{EM}} = 7$ grid points for the SOC to determine a set of weight for the recuperation torque estimation at deceleration stages. We use the identification data set, as described in section 2.1.1, to find an optimal set of weights according to equation (11). However, only data points at deceleration states ($T_{\mathrm{t},k} < 0$) are used for the identification. While the identification data already contains a measured SOC value for every single operating point, it is unknown at this stage of the prediction approach. Compared to other vehicle states, the SOC can be assumed to change significantly less dynamically. Therefore, the previous SOC $s_{\mathrm{c},k-1}$ is used for the recuperation torque estimation. As the braking torque dissipates from the system, it is not further considered for the energy demand prediction.

Driving State. At driving state, the torque distribution mainly depends on the required total drive torque and the vehicle speed. In addition, we assume that the total required drive torque is always fully distributed between electric motor and combustion engine. This allows to define r_k as a distribution ratio between electric motor torque $T_{\mathrm{EM},k}$ and combustion engine torque $T_{\mathrm{CE},k}$ by:

$$r_k = \frac{T_{\mathrm{CE},k}}{T_{\mathrm{t},k}} = \frac{T_{\mathrm{CE},k}}{T_{\mathrm{CE},k} + T_{\mathrm{EM},k}}. \tag{13}$$

In order to determine the torque distribution behavior at driving states, we declare

$$r_k(T_{\mathrm{t},k}, \overline{v}_k) = \sum_{i=1}^{M_{\mathrm{r}}} \sum_{j=1}^{N_{\mathrm{r}}} w_{\mathrm{r},i,j} \Phi_i(T_{\mathrm{t},k}, \xi_i) \Phi_j(\overline{v}_k, \eta_j), \tag{14}$$

and define $M_{\mathrm{r}} = 11$ grid points for the total torque and $N_{\mathrm{r}} = 8$ grid points for the vehicle speed. We use the identification data set as described in section 2.1.1. As the torque distribution is additionally affected by the SOC, we determine separate optimal weight sets for five different SOC-ranges.

2.2 Electric Power Train

Electric Motor. To model the energy demand of the electric part of the power train, we derive the motor's mechanical power $P_{\mathrm{m,EM},k}$ from its torque $T_{\mathrm{EM},k}$ and rotational drive shaft speed $n_{\mathrm{d},k}$, according to (Binder, 2018), as follows:

$$P_{\mathrm{m,EM},k} = 2\pi \cdot T_{\mathrm{EM},k} \cdot n_{\mathrm{d},k}, \tag{15}$$

where $n_{\mathrm{d},k}$ results from equation (10). In contrast to the gearbox and the torque distribution, characteristic diagrams are usually available for the vehicle's drives. The energy demand of the electric motor depends on it's electrical power $P_{\mathrm{el,EM},k}$, which is represented by the sum of mechanical power $P_{\mathrm{m,EM},k}$ and the power loss $P_{\mathrm{l},k}$:

$$P_{\mathrm{el,EM},k} = P_{\mathrm{m,EM},k} + P_{\mathrm{l},k}. \tag{16}$$

The power loss $P_{\mathrm{l},k}$ can be obtained by the interpolation of a characteristic diagram for given values of the rotational drive shaft speed $n_{\mathrm{d},k}$, the motor torque $T_{\mathrm{EM},k}$ and the voltage $U_{\mathrm{EM},k}$ that is applied to the motor. In order to determine the motor voltage at this stage of the prediction approach, we assume $U_{\mathrm{EM},k}$ to be a bi-quadratic function of the SOC $s_{\mathrm{c},k-1}$ and the motor torque $T_{\mathrm{EM},k}$ as follows:

$$\begin{aligned} U_{\mathrm{EM},k}(s_{\mathrm{c},k-1}, T_{\mathrm{EM},k}) = {} & p_{U_{\mathrm{EM}},1} \\ & + p_{U_{\mathrm{EM}},2} \cdot s_{\mathrm{c},k-1}^2 + p_{U_{\mathrm{EM}},3} \cdot s_{\mathrm{c},k-1} \\ & + p_{U_{\mathrm{EM}},4} \cdot T_{\mathrm{EM},k}^2 + p_{U_{\mathrm{EM}},5} \cdot T_{\mathrm{EM},k}. \end{aligned} \tag{17}$$

Using a least square algorithm, we find an error minimizing parameter set $\boldsymbol{p}_{U_{\mathrm{EM}}}$ based on measured motor voltage values within the identification data, described in section 2.1.1. Having an approximation of the motor voltage, according to (Binder, 2018), the motor current can be derived from the electrical power as follows:

$$I_{\mathrm{EM},k} = \frac{P_{\mathrm{el,EM},k}}{\sqrt{3} \cdot U_{\mathrm{EM},k} \cdot p_{I_{\mathrm{EM}}}}. \tag{18}$$

As the power factor $p_{I_{\mathrm{EM}}}$ (also known as $\cos\phi$) is unknown for the electrical motor of our test vehicle, it is identified, using a least square algorithm based on measured motor current values within the identification data described in section 2.1.1.

Battery. Finally, we model the battery of the electric power train. According to (Elgowainy, 2021) the amount of energy $E_{\mathrm{B},k}$, that is extracted from or supplied to the battery, can be determined by:

$$E_{\mathrm{B},k} = U_{\mathrm{B},k} \cdot I_{\mathrm{B},k} \cdot \Delta t_k. \tag{19}$$

While the time interval Δt_k between two operation points can be derived from the input values Δd_k and $\overline{v}_k$, the battery's voltage $U_{\mathrm{B},k}$ and its current $I_{\mathrm{B},k}$ are unknown. However, the current at the battery mainly depends on the motor current. We describe this dependence by defining a second order polynomial function:

$$I_{\mathrm{B},k} = p_{I_{\mathrm{B},1}} \cdot I_{\mathrm{B},k}^2 + p_{I_{\mathrm{B},2}} \cdot I_{\mathrm{B},k} + p_{I_{\mathrm{B},3}}, \tag{20}$$

in which an optimal parameter set $\boldsymbol{p}_{I_{\mathrm{B}}}$ is to be found, by using a least square algorithm, based on measured battery current values within the identification data set, as described in section 2.1.1. Depending on the battery current $I_{\mathrm{B},k}$ and the motor voltage we define the battery voltage $U_{\mathrm{B},k}$ by

$$U_{\mathrm{B},k} = U_{\mathrm{EM},k} + p_{U_{\mathrm{B}}} \cdot I_{\mathrm{B},k}, \tag{21}$$

and find the parameter p_{U_B} also by using a least square algorithm, based on measured battery voltage values within the identification data set. To determine the resulting SOC $s_{c,k}$, at the current operation point k, we relate $E_{B,k}$ to the total effective energy content of the battery $E_{t,eff}$ and add it to the SOC of the previous operation point $s_{c,k-1}$ as follows:

$$s_{c,k} = s_{c,k-1} + \frac{U_{B,k} \cdot I_{B,k} \cdot \Delta t_k}{E_{t,eff}}. \quad (22)$$

2.3 Combustion Engine

For a combustion engine the fuel rate $\dot{Q}_{g,k}$ for an operation point k can usually be derived from a characteristic diagram which is specified by the manufacturer. In order to derive the correlating energy demand $E_{CM,k}$ from this consumption and thus to combine it with the energy demand of the electric power train part $E_{B,k}$, the heating value of gasoline H_g is used as follows:

$$E_{CM,k} = \dot{Q}_{g,k} \cdot \Delta t_k \cdot H_g, \quad (23)$$

where Δt_k represents the past time between operation point $k-1$ and k.

3 VALIDATION RESULTS

Using the prediction approach presented in section 2 the energy demand of both engines can be determined based on route data and velocity values. To validate this approach, the data set described in section 2.1.1 is split into 6 parts. For an evaluation of the prediction accuracy we perform a 6-fold cross validation, in which 6 times 5 different data set parts are used for the identification procedure, while the remaining part is preserved for validation.

The required elevation profiles for the validation drive sequences are obtained by using a HERE routing API (HERE Maps, 2021) on the sequences' GPS values. Based on the measured vehicle speed v^*, and the obtained elevation h^*, the energy demand is determined separately for each validation drive sequence using the presented approach. Thereby, only the first measured SOC value of a drive sequence is used, while hereafter the prediction approach relies on SOC values predicted in previous steps. Thus, the remaining SOC measurements are only used for evaluation purposes. In order to asses the prediction accuracy, a root mean square error is determined between predicted and measured values. This error value is calculated for each of the 6 different validation data sets within the 6-fold cross validation procedure and than averaged.

In addition, the prediction behavior of the single power train component models is evaluated and visualized on a data set independent test drive sequence, to analyze the error propagation through the prediction approach. For this purpose, figure 2 shows the vehicle speed and the elevation profile for the first kilometer of the test drive sequence.

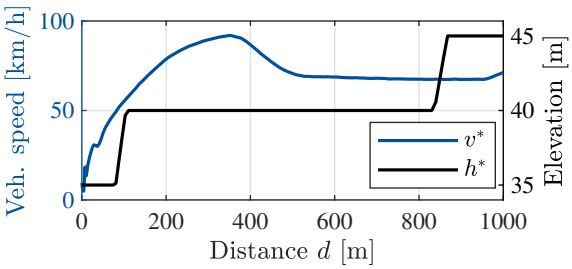

Figure 2: Vehicle speed and elevation profile.

Based on this input data, the transmission factor is predicted, as described in section 2.1.1, and compared to the actual transmission factor, which is calculated from the measured power train speed and the vehicle speed, according to equation (10). While figure 3 illustrates this comparison for the test drive sequence, the averaged root mean square error results to 0.407 for the 6-fold cross validation on the entire data set. The transmission factor's value range of our test vehicle extends from 2.44 for the sixth gear to 13.76 for the first gear. The predicted transmission factor values i_t show a reasonable fit for the test drive. However, the gearbox-related staged transmission behavior, during the dynamic acceleration stage, can only be predicted approximately.

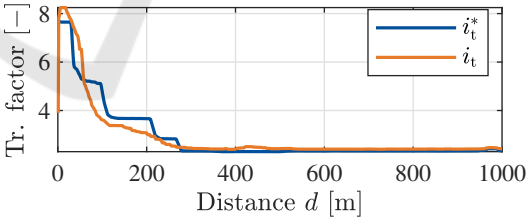

Figure 3: Transmission factor prediction and measurement.

In order to illustrate the effect of the predicted transmission factor, figure 4 shows the i_t-based prediction of the total power train torque T_t, compared to the actual measured value T_t^*. The comparison shows that even in areas where the transmission factor is not fitting properly, such as between 100 m and 200 m, the total torque prediction proves an adequate behavior. However, an occurring peak of high torque at 65 m is not met after a short interruption in the acceleration procedure (see figure 2). The averaged root mean square error on the validation data results to 27.19 Nm in a value range for the total torque from −220 Nm to

250 Nm.

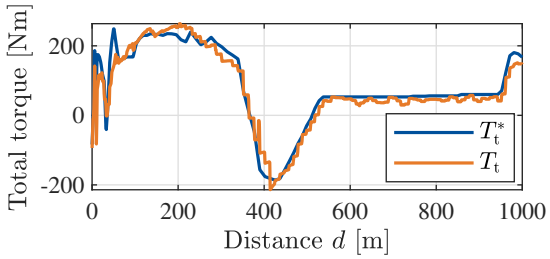

Figure 4: Total torque prediction and measurement.

The torque distribution, relying on T_t, is evaluated by comparing each engine's torque, calculated by using the predicted distribution ratio r according to equation (13), with measured engine torque values. The 6-fold cross validation on the total data set leads to an averaged root mean square error of 23.11 Nm for the electric motor torque and 17.33 Nm for the combustion engine torque. Figure 5 shows the predicted combustion engine torque T_{CE} as well as the predicted torque of the electric motor T_{EM} compared to the measured values T_{CE}^* and T_{EM}^* for the test drive sequence. Both predictions illustrate a reasonable fit. However, there are two areas to be pointed out. First, the early peaks of the measured combustion engine torque, at 20 m and at 70 m, are not met. Here, the engine was switched on shorty, which could not be predicted. This mismatch can be traced to the incorrect total torque determination in this areas (see figure 4). Second, in the area from 140 m to 180 m the torque distribution is also inaccurate. It can be seen that the torque is predicted to be applied by a combination of both engines, while the measured values indicate that the combustion engine drives the vehicle all by itself.

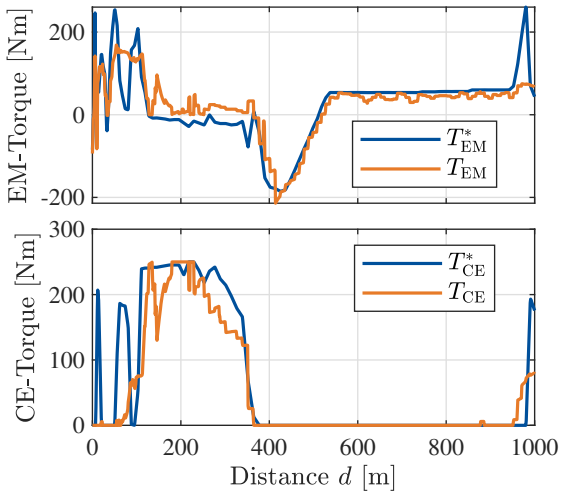

Figure 5: Prediction and measurement of engine torques.

The partly higher errors in predicting the torque distributions are probably caused by the simplification of assuming that the procedure of distributing the required drive torque is only depending on SOC and vehicle speed. Actually, this task is performed by a complex control algorithm that relies an many additional internal power train states, such as engine temperature. Furthermore, the distributing behavior is not only depending on the current operation point, but also on previous states. Thus, even if the current operation point indicates, that the torque can be applied by the electric motor only, the combustion engine might be still supporting. This can be due to higher torque requests in previous operation points and a delayed shutdown behavior. However, this and other influences can not be considered in the torque distribution model, as the purpose of the prediction approach is to be applied within optimization algorithms. These algorithms neither propagate previous states nor detailed internal power train values.

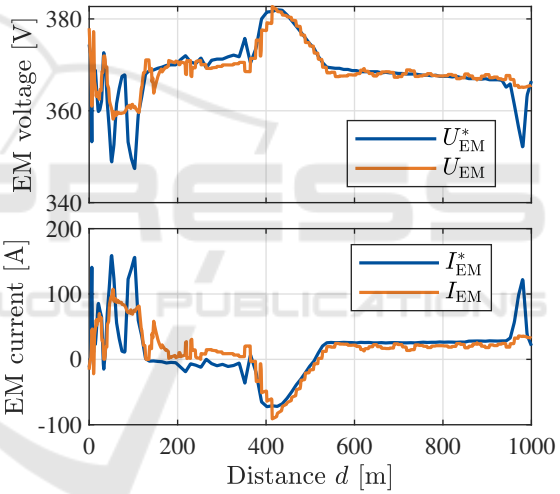

Figure 6: Prediction and measurement of current and voltage at the electric motor.

Based on the electric motor torque, the prediction of the electric motor's current and voltage are evaluated. Figure 6 shows the predicted motor current I_{EM} and the voltage U_{EM} where the propagation of the torque prediction errors are evidently reflected. The voltage root mean square error results to 2.93 V, in a value range of 320 V to 400 V. The root mean square error for the motor current is determined as 16.83 A, for occurring values between −100 A and 200 A. However, these error dimensions are caused by the preceding errors in predicting the motor torque values. When validating the motor voltage and current prediction based on measured torque values T_{EM}^*, the root mean square errors can be found as 1.74 A for the motor current and 1.69 V for the motor voltage.

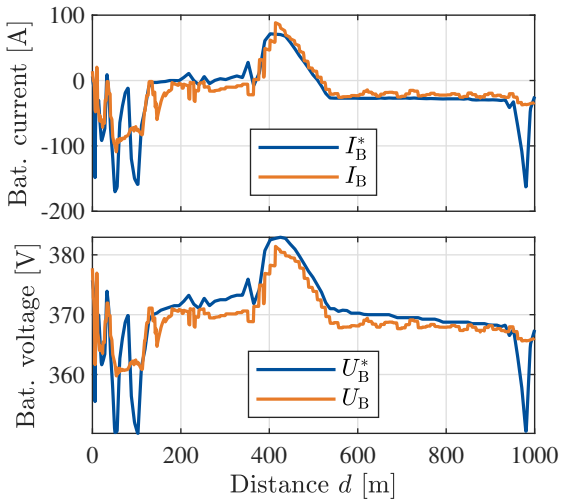

Figure 7: Prediction and measurement of current and voltage at the battery.

A similar dependence on prediction errors for the electric motor torque is indicated by the two predicted battery states current I_B and voltage U_B in figure 7. Here, a root mean square error of 16.75 A is determined for the battery current while this value equals 2.7 A when validating the prediction based on measured electric motor torque values T_{EM}^*. For the battery voltage a root mean square error is found to equal 3.13 V on a predicted electric motor torque and results to 0.99 V for measured torque values.

Finally, the prediction of the required SOC is evaluated. For this purpose, the SOC s_c is determined, based on previously predicted states of the electrical power train, as described in section 2.2. Figure 8 shows the comparison of s_c with measured values s_c^* for the selected test drive sequence. It is indicated that the preceding inaccuracies, in particular for the torque peaks mentioned above, are not affecting the SOC prediction too much. The predicted values s_c indicate a reasonable fit. However, deviating torque predictions, persisting over a longer distance, are reflected in the SOC prediction, as the area between 200 m and 400 m shows. Within the validation procedure the root mean square error for the SOC prediction is found to equal 0.91 %. A validation of the SOC

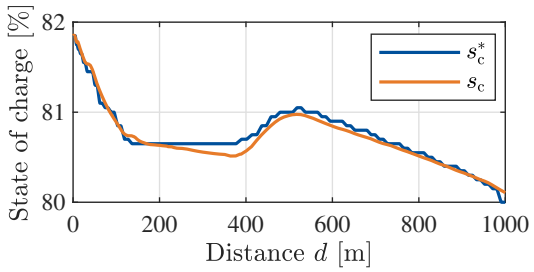

Figure 8: State of charge prediction and measurement.

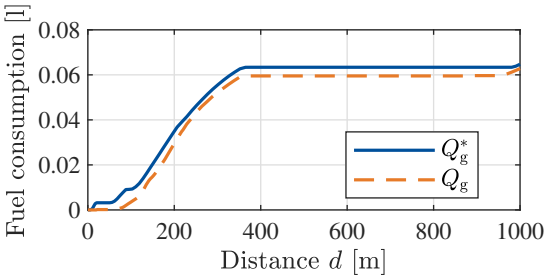

Figure 9: Prediction and measurement of the required amount of fuel.

prediction, based on measured electric motor torque values, leads to a root mean square error of 0.84 %.

Regarding the combustion engine part of the power train, the prediction of the required amount of fuel is validated. Figure 9 shows the comparison of the predicted Q_g and the measured fuel consumption Q_g^* for the test drive sequence. Here, the impact of the not predicted combustion engine torque peaks at 20 m and 70 m (cf. figure 5) forms out. The measured values increase sharply, due to the engine's switch-on process, which usually requires a relatively high amount of fuel, compared to its normal operation. This results in a remaining gap between the predicted and the measured fuel consumption. The torque deviations in the areas 140 m to 180 m and 260 m to 350 m are less effecting the consumption prediction, as for the corresponding operating points the specific fuel requirements do not differ as much. The validation procedure leads to a root mean square error of 0.05 liters when relying on the predicted torque distribution, while this error value equals 0.02 liters based on combustion engine torque measurements.

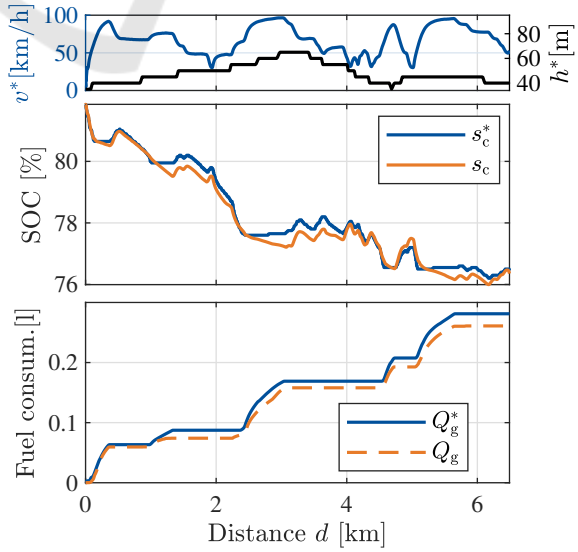

Figure 10: SOC and fuel prediction for the entire test drive sequence compared to measurements.

In order to outline the behavior of the prediction approach over a longer distance, figure 10 illustrates the SOC and fuel consumption prediction for the entire test drive sequence of 6.5 km.

4 CONCLUSION

In this paper, an approach is presented to predict the energy demand of a hybrid electrical vehicle, based on route data and speed values. The approach is build to be suitable for an application within optimization algorithms, as it only relies on input data for a single transition between two operation points. The prediction procedure is composted by a series of individual models that represent the behavior of the single power train components and can be described as follows.

For given speed and elevation values in two consecutive route points, the required drive torque at the wheels is calculated using a longitudinal vehicle dynamic model. Further, a gearbox model is build and identified to estimate the transmission behavior, based on the wheel torque and vehicle speed. In order to determine which part of the required total drive torque will be applied by the individual drives, a model is build to estimate a torque distribution ratio, based on the total drive torque, the vehicle speed and the previous state of charge. Having the separate torque values, the combustion engine's required amount of fuel can be derived from a characteristic diagram. For the electric part of the power train, the current and the voltage are estimated and used within a battery model to determine the required electric energy.

A data set of 525 driven kilometers is created to identify and validate the prediction approach on a Volkswagen Golf VII GTE. Using drive sequences of 5 to 7 km within a 6-fold cross validation procedure, an averaged root mean square error of 0.91 % can be determined for the prediction of the state of charge. Regarding the prediction of the amount of fuel required by the combustion engine, this error value results to 0.05 liter. The main part of prediction inaccuracies can be attributed to the estimation of the single torques, to be applied by the individual engines. In dynamic driving situation, in which both engines are required, the estimation approach is not always capable to predict the correct distribution of the required total drive torque. This might be approved by a more complex model or by including the current acceleration, when estimating the torque distribution. In addition, future work will investigate data-driven methods, such as neural networks, for their ability of estimating the energy demand. Other advantages can be assumed in involving more than one previous operation point, if they are given within the target application of the prediction approach.

REFERENCES

Bellman, R. E. (2003). *Dynamic programming*. Dover Publications, Mineola, N.Y.

Binder, A. (2018). *Elektrische Maschinen und Antriebe: Grundlagen, Betriebsverhalten*. Springer Berlin Heidelberg, Berlin, Heidelberg, 2. aufl. 2017 edition.

Elgowainy, A., editor (2021). *Electric, Hybrid, and Fuel Cell Vehicles*. Springer eBook Collection. Springer New York and Imprint Springer, New York, NY, 1st ed. 2021 edition.

Fiori, C., Ahn, K., and Rakha, H. A. (2018). Microscopic series plug-in hybrid electric vehicle energy consumption model: Model development and validation. *Transportation Research Part D: Transport and Environment*, 63:175–185.

Freuer, A. (2016). *Ein Assistenzsystem für die energetisch optimierte Längsführung eines Elektrofahrzeugs*. Springer Fachmedien Wiesbaden, Wiesbaden.

HERE Maps (2021). https://www.here.com/platform. (last viewed 03/11/2022).

Hülsebusch, D. (2018). *Fahrerassistenzsysteme zur energieeffizienten Längsregelung - Analyse und Optimierung der Fahrsicherheit*. PhD thesis, Karlsruher Institut für Technologie.

Mitschke, M. and Wallentowitz, H., editors (2004). *Dynamik der Kraftfahrzeuge*. VDI-Buch. Springer Berlin Heidelberg, Berlin, Heidelberg and s.l., vierte, neubearbeitete auflage edition.

Nelles, O. (2001). *Nonlinear System Identification: From Classical Approaches to Neural Networks and Fuzzy Models*. Springer eBook Collection. Springer, Berlin and Heidelberg.

Pitanuwat, S., Aoki, H., IIzuka, S., and Morikawa, T. (2019). Development of hybrid vehicle energy consumption model for transportation applications—part ii: Traction force-speed based energy consumption modeling. *World Electric Vehicle Journal*, 10(2):22.

Radke, T. (2013). *Energieoptimale Längsführung von Kraftfahrzeugen durch Einsatz vorausschauender Fahrstrategien*. Karlsruher Schriftenreihe Fahrzeugsystemtechnik. KIT Scientific Publishing.

Rosenzweig, J. and Bartl, M. (2015). A review and analysis of literature on autonomous driving. *The Making of Innovation*, pages 1–57.

Sajadi-Alamdari, S. A., Voos, H., and Darouach, M. (2020). Ecological advanced driver assistance system for optimal energy management in electric vehicles. *IEEE Intelligent Transportation Systems Magazine*, pages 92–109.

Zhang, F., Wang, L., Coskun, S., Pang, H., Cui, Y., and Xi, J. (2020). Energy management strategies for hybrid electric vehicles: Review, classification, comparison, and outlook. *Energies*, 13(13):3352.